Available online at www.sciencedirect.com

jmr&t Journal of Materials Research and Technology

journal homepage: www.elsevier.com/locate/jmrt

Original Article

Mechanical behavior of additively and conventionally manufactured 316L stainless steel plates joined by gas metal arc welding

Moritz Braun [a,*], *Jan Schubnell* [b], *Ardeshir Sarmast* [b], *Harihara Subramanian* [b], *Lutz Reissig* [b], *Felix Altenhöner* [c], *Shahram Sheikhi* [c], *Finn Renken* [d], *Sören Ehlers* [a]

[a] *German Aerospace Center (DLR), Institute of Maritime Energy Systems, Max-Planck-Straße 2, D-21502 Geesthacht, Germany*

[b] *Fraunhofer Institute for Mechanics of Materials, Woehlerstr. 11, D-79108 Freiburg, Germany*

[c] *University of Applied Science Hamburg, Institute of Materials Science and Joining Technology, Berliner Tor 13, D-20099 Hamburg, Germany*

[d] *Hamburg University of Technology, Institute for Ship Structural Design and Analysis, Am Schwarzenberg-Campus 4C, D-21073 Hamburg, Germany*

ARTICLE INFO

Article history:
Received 14 February 2023
Accepted 12 March 2023
Available online 21 March 2023

Keywords:
Fatigue strength
Additive manufacturing
Gas metal arc welding
Weld geometry
Residual stress relaxation
Process-microstructure-property relation

ABSTRACT

Combining several additive manufactured (AM) parts to larger parts by welding may be required due the limited building volume of powder bed AM methods. Laser powder bed fusion (LPBF) has a great potential because it enables the production of nearly full-density components through AM processes; however, additional residual stresses and production defects are induced by LPBF. These residual stresses affect the residual stress state of welded AM parts. In combination with the production related defects, both alter the mechanical and—in particular—the fatigue behavior of these welded joints. In this study, various tests are performed to characterize the butt joints of 316L AM steel plates made by gas metal arc welding. To this goal, joints are produced with weld seams parallel and vertical to the layer orientation of AM plates. The results are compared to joints of conventionally rolled steel plates produced with the same welding parameter. The residual stress states in initial (unloaded) condition and after cyclic loading were determined by X-ray diffraction techniques for AM and rolled plates. Complex residual stress states were determined at the welds made of AM steel plates compared to the welds made of rolled steel plates; however, the residual stress level in the heat affected zone of the butt-welded AM steel plates was similar to the welds made of hot-rolled steel plates. After cyclic loading with a high load level, high residual stress relaxations were observed in the parent materials. The fatigue design curve for butt joints from international standards is exceeded by all three test series, but the fatigue strength of the butt joints made by LBPF and hot rolling vary significantly. This is thought to be related to differences between the AM and conventional joints in microstructure, static strength, residual stress level, and small crack-like defects that partially interact with stress concentrations at the weld transition.

* Corresponding author.
E-mail address: moritz.braun@dlr.de (M. Braun).

https://doi.org/10.1016/j.jmrt.2023.03.080

1. Introduction

Additive manufacturing (AM) and laser powder bed fusion (LPBF) has seen a rapid increase for many applications in recent years. Thus, there are still technical limitation with respect to industrial applications. An important aspect is the limited building volume of the LPBF process. Thus, the joining of different additively manufactured parts or combinations with traditionally manufactured components such as wrought materials makes it possible to increase the volume of such parts and components [1]. Welding of AM parts is thought to be a good option to join AM parts to larger structures, but there are currently not many investigations on the mechanical properties of welded AM parts. In particular, fatigue strength of welded AM parts in comparison with joints of wrought material is rarely investigated. The reason for this unknown influence is related to the interaction of additional welding-related heat input and properties of the AM parts, microstructure, imperfections, including surface topology, and residual stress states [2].

The fatigue strength of AM parts—including stainless steels such as 316L—has been investigated in the past; however, as to the best knowledge of the authors a thorough investigation of the fatigue behaviour of AM parts joined by gas metal arc welding (GMAW), including a comparison with rolled sheet material, has not been performed yet.

Previous studies on the joining of LPBF components made of the alloy 316L have mainly focused on laser welding or tungsten inert gas welding. So far, there is a lack of extensive investigations on GMAW of LPBF components, despite the wide application of this process in industry. Current developments enable higher quality welds, with better control of heat input (pulse) and arc stability (pulsed), which makes it a very cost-effective welding process.

From previous studies, it is known that the fatigue strength of plain specimens without notches and similar surface roughness (e.g., after milling) is similar for specimens conventionally manufactured and by LPBF, but that the fatigue strength is different for notched components, see [3–5]. This was attributed to small defects caused by the LPBF process. Similarly, differences in fatigue strength are expected for components made by AM and conventional manufacturing processes. Hence, this study investigates the mechanical behaviour of butt joints of 316L LPBF and rolled sheet material. To this goal, the following aspects are investigated and presented.

- Welded joints from 316L LPBF and rolled sheet material are characterised by a microstructure comparison, residual stress measurements, weld geometry measurements, static and cyclic mechanical properties such as fatigue strength, stress–strain behaviour and Charpy impact toughness.
- The relaxation of residual stresses under cyclic loading is investigated to determine the degree of residual stress relaxation and the cyclic stabilized residual stress state.
- Fracture surface investigations by scanning electron microscopy is used to investigate whether fatigue cracks are caused by defects of the LPBF process or by the stress concentration at weld toes

The following section will offer a short overview of current state-of-the-art research on welding of AM parts, followed by the characterisation of butt joints of 316 LPBF and rolled sheet stainless steel made by gas metal arc welding. Finally, the results of the fatigue tests are discussed based on the extensive characterisation of the welded joints.

2. State of the art on welding of additively manufactured parts

Welding of additively manufactured parts can be a fast and inexpensive solution for various tasks such as the replacement of damaged components or to assemble larger components from smaller AM parts, because LPBF of entire assemblies is typically too expensive to be economically feasible. The build size limitations and high production costs of LPBF make it competitive for smaller, highly complex components, while the less complex elements of an assembly are manufactured traditionally. This leads to scenarios where joining is required to form the final product. For example, Geisen et al. [6] presented an integrated weld preparation designs for the joining of LPBF and traditional pipe components made of Inconel 625 by tungsten inert gas welding.

Welding of AM parts is, however, not straightforward and might require additional welding tests to determine suitable welding process parameters compared to welding of rolled sheet material. Brunner-Schwer et al. [7] performed bead-on-plate laser beam welding tests on plates manufactured by LPBF on Inconel 718. It was found that the weld geometry differed from the wrought material and that the weld profile is a function of the LPBF building direction and laser power. In a similar study, Jokisch et al. [8] investigated laser welding of LPBF Inconel 625 and Inconel 718 tubes. They found that no continuous good welding quality could be accomplished due to welding defects caused by capillary instabilities. In addition, both studies recommended to perform heat treatment prior to welding to improve the weld quality.

To weld AM stainless steels parts for marine application, further properties such as corrosion behavior needs to be taken into account. Sampath et al. [9] therefore examined the technical feasibility of using LPBF printed 316L stainless steel parts as a replacement for legacy pipeline assets (e.g. casted valve body, complex shaped pipes, heat exchanger tubular structures). It was found that the corrosion susceptibility of the LPBF 316L is lower than the wrought material in tungsten

Table 1 – Chemical composition of the base metals and wire (wt%) [15].

	Cr	Ni	Mo	Mn	Si	C	N	Nb	P	Fe
LPBF 316L	16.77	11.98	2.27	0.90	0.55	0.015	0.070	0.011	0.009	67.22
Hot-rolled 316L	16.85	9.63	1.89	1.21	0.28	0.016	0.041	0.027	0.017	69.36
Wire 316LSi	18.65	11.64	2.29	1.76	0.65	0.026	0.035	0.016	0.003	64.62

inert gas welded parts. In addition, due to its good weldability LPBF 316L retains high strength and ductility.

Furthermore, fatigue strength of 316L steel welds are strongly related to their individual residual stress state [10]. Tensile residual stress were created in the longitudinal direction after deposition of the material [11]. Fluctuations in local residual stresses in direct energy deposited 316L were determined [12]. In the case of powder bed fusion additive manufacturing, these residual stresses could be as high as the bulk material yield strength or even excessive of that [13]; however, it was shown that the building direction has a high influence on yield strength and other mechanical properties of LPBF 316L [14]. Another work investigated the effect of AM process parameters and component geometry on the residual stress formation on the surface of the additively manufactured 316L specimens and showed that the residual stresses are compressive in depth of an additive manufacturing 316L component and tensile near its surface [13]. A former study at butt joints made of different AM and hot-rolled 316L sheets has shown a high difference of the residual stress state at the different parent materials [15]. Comparable high tensile residual stresses were determined at the surface depending on the building direction, while compressive residual stresses close to the surface were determined in hot-rolled 316L steel sheets; however, the residual stresses were similar close to the welded joint. It was assumed that this is related to the relaxation of process-induced residual stresses in the parent material during heating and cooling while welding.

Based on the aforementioned investigations, it is assumed that the residual stress state and imperfections affects the fatigue life of welded joints made of conventionally hot-rolled and LPBF 316L steel sheets. In addition, the interaction between welding residual stresses and the stress state of the steel sheets after hot rolling or LPBF under cyclic loading and their influence on the fatigue performance of welding joints is unknown. The aim of this study is to determine the mechanical behavior of butt joints made of LBPF 316L and conventionally hot-rolled sheets by gas metal arc welding. Also, the residual stress state after joining and after cyclic loading is investigated depending on the manufacturing process of the parent material. In addition, the butt joints are characterized by a microstructure comparison, weld geometry measurements, stress–strain behaviour and Charpy impact toughness. Finally, fracture surface investigations by scanning electron microscopy are used to investigate whether fatigue cracks are caused by defects of the LPBF process or by the stress concentration at weld toes.

3. Specimen characterization and manufacturing

3.1. *Description of specimen manufacturing*

To enable a meaningful comparison, 316L steel was used as powder for the LPBF plates, as hot-rolled steel sheets. A typical wire for joining 316L materials was used as filler material (316LSi). The chemical compositions are given in Table 1. Mechanical properties of the rolled sheet material and for similar AM parameters were previously investigated by Braun et al. [14] and Taghipour et al. [16]. In total, three different parent material conditions were used for the welding, see Fig. 1(c): Hot-rolled, LBPF welded parallel to the building direction (AM parallel), LBPF welded vertical to the building direction (AM vertical). The mechanical properties of the parent material differ in each direction, which were determined by Braun et al. [14], are summarized in Table 2.

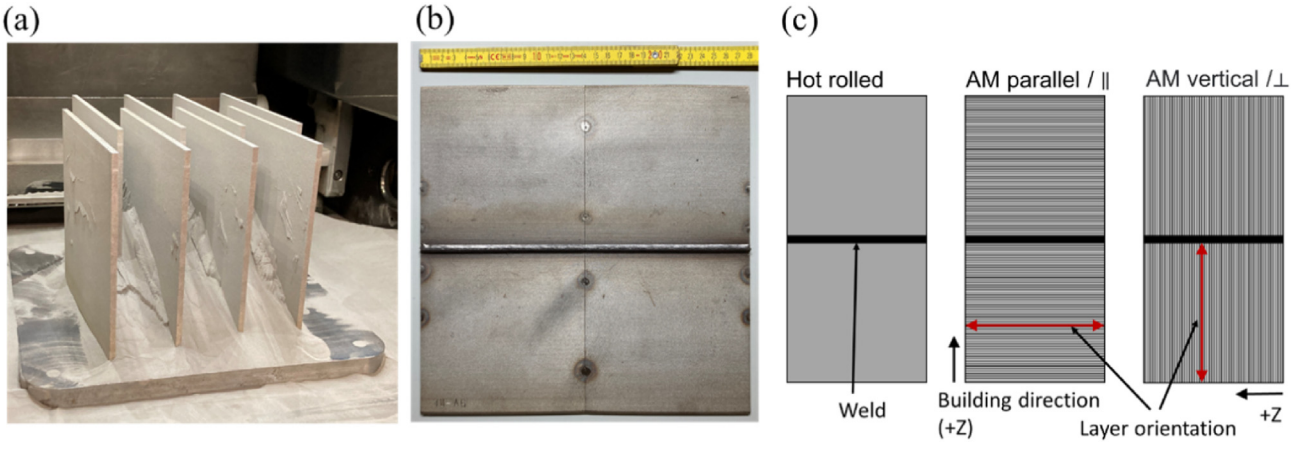

Fig. 1 – (a) LPBF manufacturing of plates; (b) specimens joined from four LPBF plates; (c) investigated conditions [15].

Table 2 – Mechanical properties of 316L depending on parent material condition (z-direction, see Fig. 1 (c)) [14].

	Young's modulus E [GPa]	Yield strength σ_{YS} [MPa]	Ultimate tensile strength σ_{UTS} [MPa]	Fracture strain ε_f [%]
Hot-rolled	174	263	589	59.2
AM vertical (building direction perpendicular to weld seam)	157	510	619	42.2
AM vertical (building direction parallel to weld seam)	163	614	727	34.2

The LPBF plates were built on a Renishaw AM 250 system perpendicular to the base plate. The dimensions of the plates are 140 mm in length and height; having a thickness of 4 mm. The scanning strategy used a rotation of 67° in the scanning direction after each layer. During the building process the chamber was filled with argon as shielding gas. The manufacturing parameters and the LPBF plates after manufacturing are displayed in Table 3 and Fig. 1(a), respectively. For each type, four plates were combined by welding, see Fig. 1(b) [15].

The plates were prepared in a Y-shape with a 1 mm 45° chamfer before welding. The edge faces of the LPBF and hot-rolled plates were ground (P320) between the butt welds. The area for the welding was cleaned with acetone afterwards. Welding was performed by gas metal arc in pulse mode with a Dinse DIX PI 400. To achieve even welding seams, the torch was assembled on an automated gantry system. The same parameters were used for all welds, which are displayed in Table 4. The base metals and welded cross-sections were assessed using stereomicroscopy. The results are presented Fig. 2.

3.2. *Micro-structural characterization*

The rolled sheet material has equiaxed grains containing twins, see Fig. 3(a) and (b). This is a typical microstructure for rolled and annealed austenitic sheets. In contrast, the LPBF 316L is characterized by individual weld beads or molten pools (Fig. 2(b) and (c)), which is related to the segregation of alloying components during the rapid solidification of the melt and the reaction of the top surface of the melt pool with the atmosphere of the pressure chamber. The resulting layer-like structure in building direction is totally different from typical austenitic microstructure—e.g., observed for the examined rolled sheet material. This leads to large elongated grains in the LPBF microstructure and thereby anisotropic mechanical properties, see [17]. The highly non-equilibrium microstructures, high density of dislocations, cellular structures, and chemical segregation of the LPBF material causes significant differences in mechanical in comparison to traditional manufacturing processes, see also [16,18,19].

Table 3 – LPBF manufacturing parameters [15].

Parameter	Unit	Value
Laser power	[W]	200
Laser scanning speed	[mm/s]	812.5
Layer thickness	[μm]	40
Hatching Distance	[μm]	110
Scanning pattern	[–]	Strips

The grain morphology of the rolled sheet and LPBF 316L samples were characterized by electron backscatter diffraction (EBSD) by Taghipour et al. [16]. The rolled sheet material is composed of equiaxed grains and twinnings without pronounced texture. The grain size is and relatively uniform with an average size of around 30 μm, see Fig. 3(a) and (b). The red lines in the grain boundary (GB) maps represent, low-angle grain boundaries (LAGBs) with a misorientation angle between 2° and 15°, whereas the black lines characterize the high-angle grain boundaries (HAGBs) with a misorientation angle higher than 15°. The microstructure features are summarized in Table 5. The microstructure of the rolled sheet sample consists to a large extend of HAGBs, see Fig. 3(b). In contrast, the microstructure of the LPBF 316L in the x-y plane—perpendicular to the building direction—is defined by columnar grains in the middle of the molten pool and fine equiaxed grains in the bottom of the molten pool, see Fig. 3(c) and (d). The majority of columnar austenite grains grow close to the building direction; yet, a small amount also grows across the deposited layers. The fraction of LAGBs in LPBF 316L in the x-y plane is higher than that of the rolled sheet material [16].

The difference in microstructure for rolled sheet and LPBF 316L leads to large difference in yield and ultimate strength with more than twice the yield strength of LPBF tensile specimens perpendicular to the building direction compared to the rolled sheet material; however, the LBPF material shows anisotropic mechanical properties and strain hardening behavior, see [16] for further information.

3.3. *Hardness measurements*

The results of the hardness measurements using HV 0.5 are presented in Fig. 4. The LPBF parent material (black and grey markers at the end of the lines in Fig. 4) has a hardness of 220–250 HV 0.5 in the range 6–7 mm from the center of the weld. The highest measured values are thus in parent material produced by LPBF process. The lowest values, at 170–190 HV 0.5, are found inside the weld metal and the adjacent HAZ.

Table 4 – GMAW welding parameters [15].

Parameter	Unit	Value
Voltage	[V]	21.5
Wire feed rate	[m/min]	7.8
Wire diameter	[mm]	1
Torch angle	[deg]	0
Travel speed	[mm/min]	600
Standoff distance	[mm]	10
Gas flow rate	[l/min]	11

Fig. 2 – (a) Hot-rolled plate: macrograph of the weld seam; (b) LPBF plate: macrograph of the weld seam and hardness measurements; (c) magnification of fusion zone, heat-affected zone (HAZ) and LPBF base metal [15].

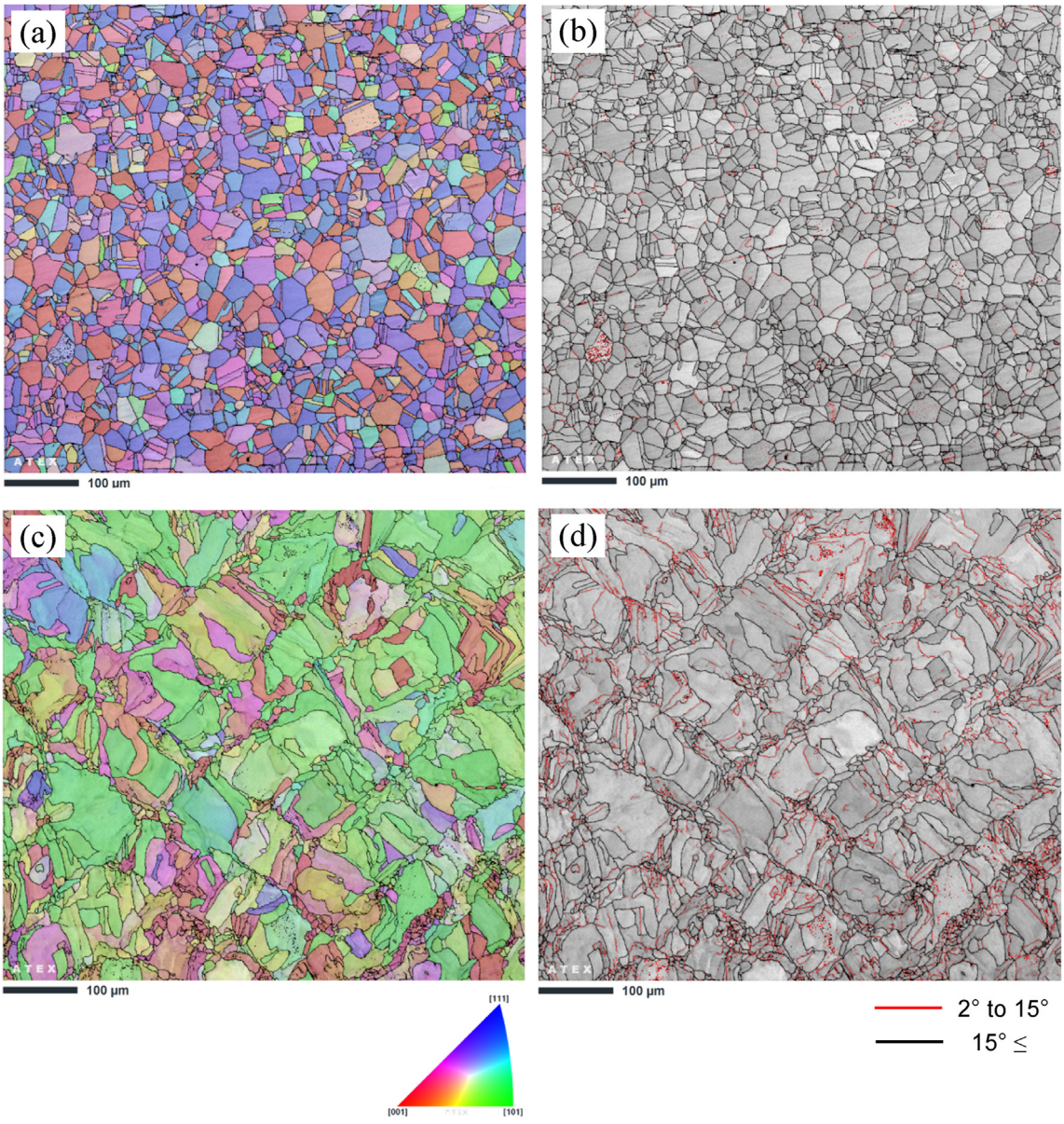

Fig. 3 – EBSD IPF (a and c) and GB (b and d) maps of the rolled sheet (a and b) and LPBF (c and d) 316L stainless steel on x-y plane (perpendicular to rolling and building direction), taken from Taghipour et al. [16].

Table 5 – Summary of microstructure features.

Material	Location	Average grain size	Average fraction of high-angle grain boundaries
Hot-rolled sheet		30 μm	95%
LPBF 316L in the x–y plane	Middle of the molten pool	100 μm	74%
	Bottom of the molten pool	25 μm	

Consequently, the area of the welded joint can be localized in the hardness curve. In addition, the area of heat influence can be recognized, which acts on both sides up to 5 mm starting from the center of the weld. The measured values of the HAZ lie between those of the base metal and the weld metal.

In the hot-rolled reference specimen, the hardness measurements are almost constant over the joint. There are no significant differences between base metal, HAZ and weld metal. The highest values in the series of measurements are in the range of 190 HV 0.5 and occur both in the weld metal and in the base metal, at a distance of 3 mm from the center of the weld. The lowest value, 164 HV 0.5, is 5.5 mm from the weld center. Although the microstructure of the base metal and weld metal differs visibly, there is only a slight variation in the hardness values.

3.4. *Charpy V-notch impact tests*

To compare the impact toughness of the test series, samples with notch location in the HAZ were performed. Due to the low thickness, specimens with reduced thickness of 2.5 mm were used. The results of the V-notch impact tests are presented in Fig. 5.

The LPBF specimens have a lower impact energy in both layer orientations (16–20 J) than the hot-rolled material (26 J). In addition, the LPBF test specimens were separated by the pendulum hammer, while the rolled test specimens were not separated. The LPBF specimens with vertical orientation absorbed the lowest notched impact and the results of the rolled test specimens agree well with literature.

3.5. *Tensile tests*

Additional tests were performed to determine the tensile strength of the butt joints after welding. Before welding, yield strength σ_{YS} and ultimate tensile strength σ_{UTS} are higher for LBPF than for the hot-rolled parent material. In contrast, the fracture strain ε_f is higher in the hot-rolled material. In Fig. 6, the results of the tensile tests performed on butt joints are presented in Fig. 6.

Again, the additively manufactured specimens show a higher yield strength than the hot-rolled reference material; however, values differ between the two layer orientations. The vertical orientation has the highest value with 456 MPa compared to 409 MPa (parallel) and 361 MPa (hot-rolled). Similarly, the ultimate tensile strengths differ as well. The LPBF and the hot-rolled tensile specimens with butt welds all failed in the weld metal. As expected, the results vary significantly between these two layer orientations of LPBF specimens. The highest tensile strengths are achieved by the LPBF vertical type with 674 MPa, while the parallel orientation showed the lowest values with in average 583 MPa. The rolled steel specimens are between the two differently oriented additive specimens with 617 MPa on average. Finally, the LPBF specimens with both layer orientations show a lower fracture strain compared to the hot-rolled material. The lowest fracture strain was obtained for the vertical orientation with 14.7%. Interestingly, the parallel orientation achieves almost twice the fracture strain of the vertical orientation with 28.3%. The hot-rolled material reached the best fracture strain with 32.4%.

In summary, the yield and ultimate tensile strength of the butt joints of LPBF material of vertical layer orientation are the highest, but the fracture strain is the lowest. For the welded hot-rolled reference specimen, the fracture strain is the highest, but the yield strength is the lowest, and the tensile strength is between the two LPBF types. For the LPBF material of parallel layer orientation, the ultimate tensile strength is the lowest, and the yield strength and fracture strain are between the other two series. In general, the results of the

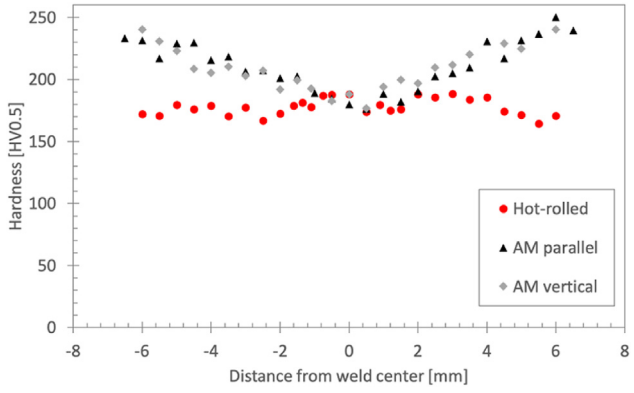

Fig. 4 – Hardness measure along a line trough the LPBF and hot-rolled 316L stainless steel welded joints.

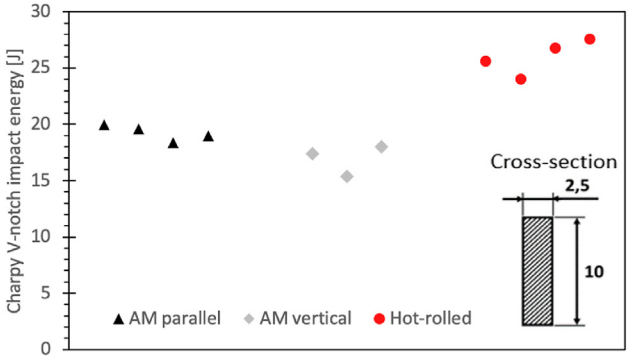

Fig. 5 – Results of Charpy V-notch impact tests of the LPBF and hot-rolled 316L stainless steel welded specimens in the HAZ.

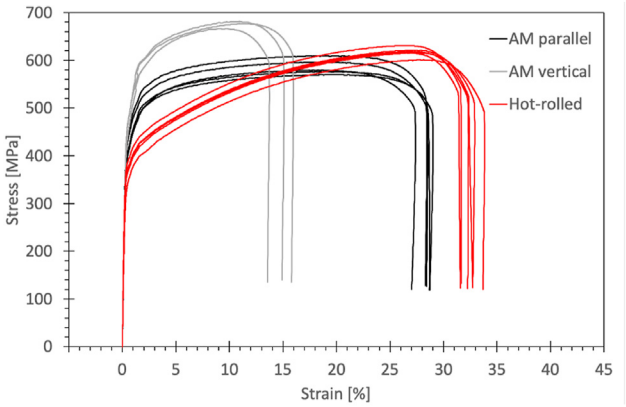

Fig. 6 – Tensile test results for the LPBF and hot-rolled 316L stainless steel welded specimens.

welded joints confirm the results from the tensile tests of the parent material. Only the tensile strength of the welded hot-rolled specimens is higher than the LPBF joints with vertical orientation. The other results confirm the order of the parent material tests.

Despite the failure of the specimens in the weld metal, an influence of the properties of the parent materials is eminent. The anisotropic behavior of the LPBF parent materials is confirmed by the tensile tests on welded joints.

4. Residual stress analysis

Previous studies have shown high differences regarding the residual stress level of different parent material conditions in AM 316L specimen [15]. It is assumed that residual stresses may have an influence on the fatigue strength of welded joints depending on their stability under fatigue loading. For this reason, the residual stress state depending on the material condition was experimentally determined after manufacturing and after fatigue loading.

4.1. *Sinψ^2-method and cos α-method*

X-ray diffraction (XRD) methods are used to determine residual stresses close to the surface. The presence of residual stresses change the lattice spacing of an unstrained crystal. A decrease or increase in the lattice spacing appears as the angular shift in position of the diffraction line according to Bragg's law. A D8 Discover laboratory x-ray diffractometer was used with a one-dimensional Lynxeye XE-T detector for the data collection. The data collection time was 2 s, and the step size was 0.04°. The measurement parameters are used from former investigations by Schubnell et al. [15] and are summarized in Table 6.

As second method for residual stress assessment the cos α-method was used. The stress analysis by the cos α-method [20] is based on a strain evaluation over the complete Debye–Scherrer-ring ($\alpha = 0–360°$) based on a 2D-detector (digital image plate). The reliability of this method in combination with the 2D-detector compared to the commonly used sinψ^2-method [21] for austenitic stainless steels was shown by Sasaki et al. [22,23] and Schubnell et al. [15] as single exposure technique (SET). The strain in circumferential direction (α-position) is measured by a shift of the diffraction angle θ_α or radius r_α. For the measurement, the detector distance to specimen L and tilt angle ψ_0 kept constant. According to the cos α-method a strain parameter ε_{a1} is defined based on four strains from $\alpha = 0°–90°$. The stress σ_φ is calculated according to equation (1) and equation (2). For detailed description of the method see by Tanaka [24].

$$\sigma_\varphi = -\frac{E}{1+\upsilon}\frac{1}{2\sin\eta\sin 2\psi_0}\frac{\partial\varepsilon_{a1}}{\partial\cos\alpha} \quad (1)$$

$$\text{with } \varepsilon_{\alpha 1} = [(\varepsilon_\alpha - \varepsilon_{\pi+\alpha}) + (\varepsilon_{-\alpha} - \varepsilon_{\pi-\alpha})]/2 \quad (2)$$

For the XRD-analysis according to the cos α-method, a diffractometer (type Pulstec μ-360) were used. The diffractometer was mounted on an industrial robot type Kuka KR3 R540. A constant sample distance of $L = 37$ mm and a constant tilt angle of $\psi_0 = 30°$ were used for all measurements. Due to less crystal planes in the measurement volume (coarse grain effect), a linear oscillation in Y-direction by ±2.5 mm was implemented. According to the recommendation of Nitschke-Pagel [25] for the XRD-measurement of welded joints, a collimator size of 1 mm was used for both methods.

4.2. *Residual stress state after welding*

The residual stress distribution around the weld at the center of the specimens is given in Fig. 7(a) and (b). The error bar in the graphs is the standard deviation taken from the sin^2 ψ- and the cos α-method. All measurements were performed on a single line at the center of the specimen. Comparable low residual stresses values between −75 MPa and 25 MPa were determined for both AM conditions in transverse direction close to the weld toe. Tensile residual stresses between 30 MPa and 110 MPa were detected in longitudinal direction in hot-rolled condition; thus, only compressive residual stresses could be determined in transverse direction in hot-rolled condition. The residual stress state around the weld shows significantly less differences in all three conditions compared to the measurements of the parent material, see Schubnell et al. [15]. No significant texture effect (orientation of the crystal planes in mainly one direction) could be determined for all material conditions. The distribution of the full width half maximum, see Fig. 7, shows nearly no differences for both AM conditions. Similar results are achieved for both evaluation methods (cos α-method and sin^2 ψ-method). The full width half maximum (FWHM) correlates with grain size and dislocation density as well as the hardness of the material [26]. As shown in Fig. 7(c), the FWHM results are similar close to the welded toe. Also, similar values of FWHM are determined for both AM conditions (AM vertical and AM parallel).

4.3. *Residual stress state after fatigue loading*

The residual stress distribution at the surface of the specimen after $N = 10{,}000$ load cycles were determined by XRD-analysis (cos α-method) to determine the degree of residual stress relaxation and the cyclic stabilized residual stress state. It is

Table 6 – Parameter for XRD-analysis taken from Schubnell et al. [15].

Parameter	Radiation	Lattice plane	E [GPa]	υ [-]	∅ [mm]	Exposure time	Measurement time
$\sin^2\psi$-method	CrK α	{311}	189	0.29	1	2.5 h	≈3 h
Cos α-method	CrK β	{220}				60 s	≈120 s

typically assumed that the residual stresses remain stable for a long period of the fatigue life after reaching $N = 10{,}000$ load cycles [27,28]. Only the residual stresses transverse to the weld were measured. One specimen per parent material condition (hot-rolled, AM parallel, AM vertical) was loaded with a load level corresponding to the upper limit in the fatigue test setup (max. nominal stress 283–289 MPa), and one specimen was loaded with a load level corresponding to the lower level (max. nominal stress 199–216 MPa). This level was chosen based on the first fatigue tests to be above the fatigue limit (no run outs).

The results are given in Fig. 8(a). As expected, a significant relaxation of the residual stresses was determined for all parent material conditions for the high load level. In

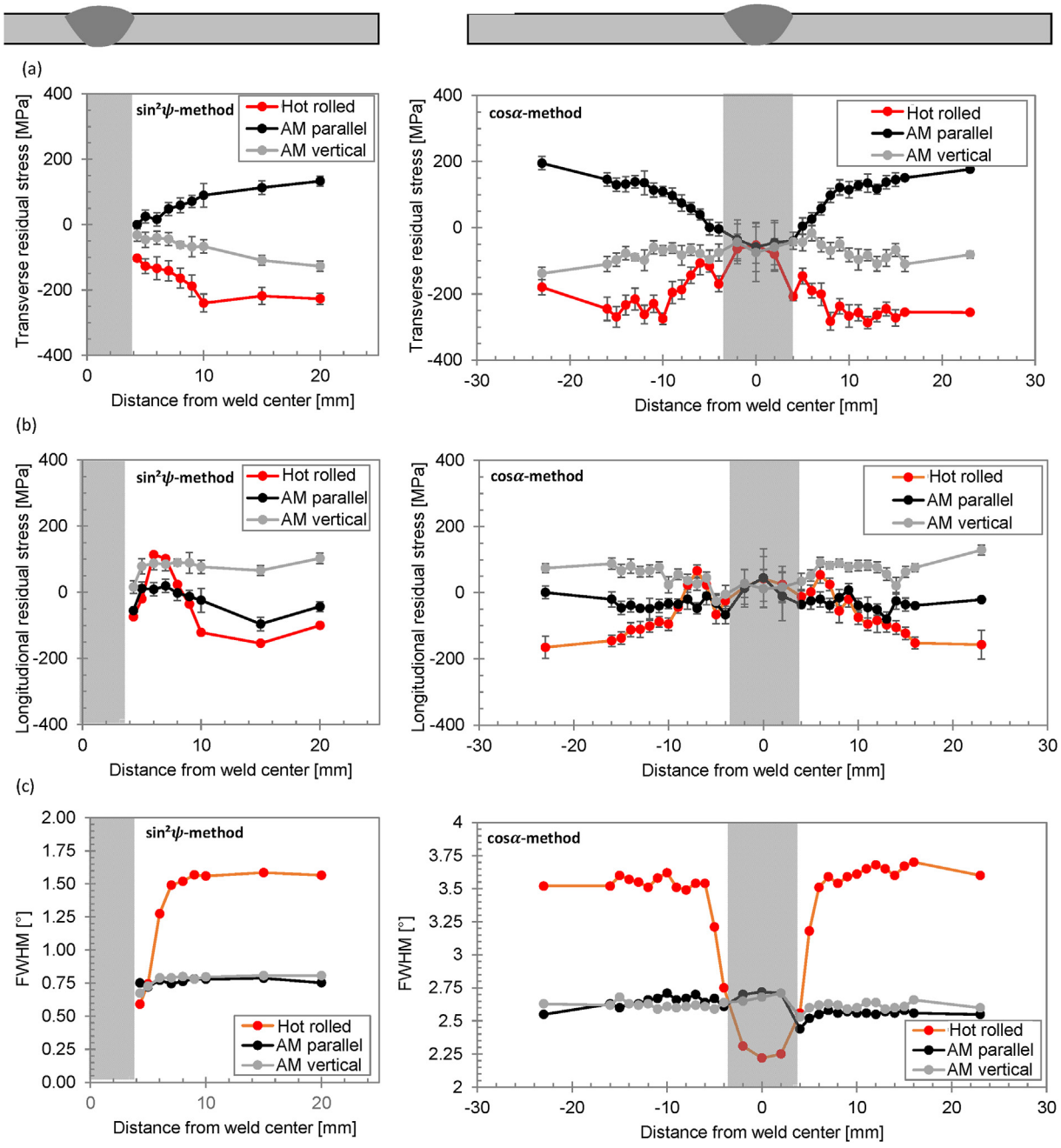

Fig. 7 – Residual stress distribution transverse (a) and longitudinal (b) from the welded joint and distribution of the full width half maximum (FWHM) (c) [15].

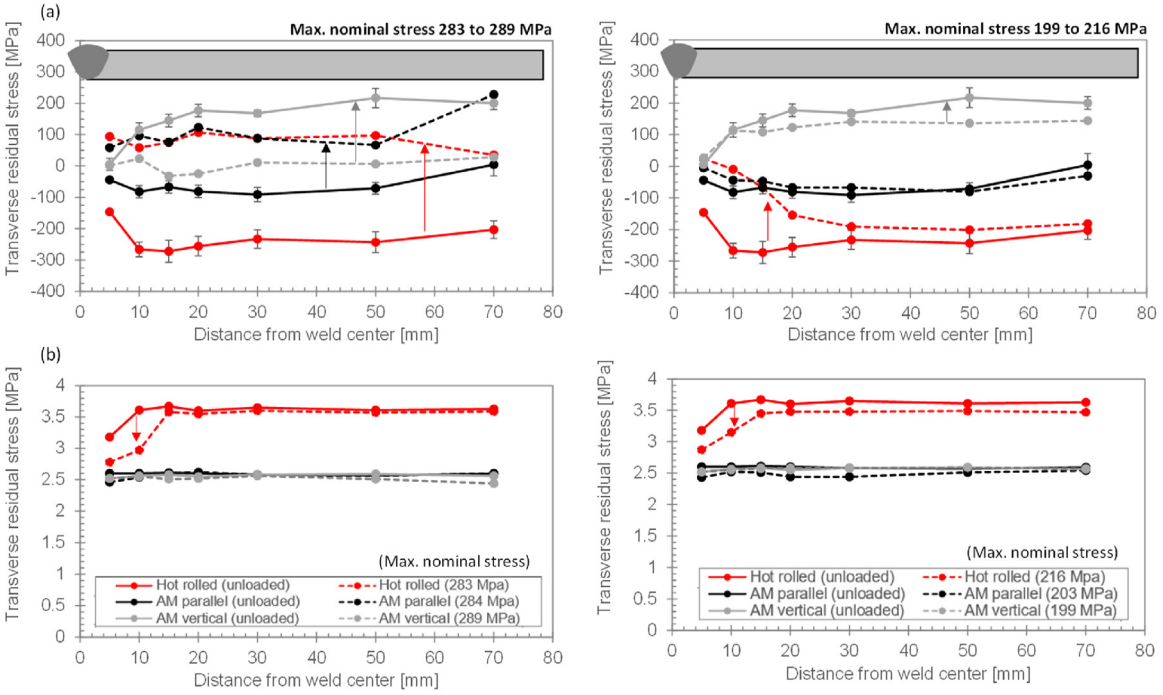

Fig. 8 – Residual stress distribution (a) and distribution of the full width half maximum (b) before and after cyclic loading.

particular, the specimen made from hot-rolled material show a significant change of the residual stresses from compression to tensile residual stress state (from in average −230 MPa–90 MPa). For the low load levels, only slight changes of the residual stresses were determined for the specimen made of AM parent material; however, for the specimen made of hot rolled parent material, a high relaxation of residual stresses was measured also for the low load level. The distribution of the FWHM before and after cyclic loading is given in Fig. 8(b). A change of the FWHM under loading may correlate with changes in the microstructural or mechanical properties (cyclic hardening or softening) [29,30]. Again, only the specimen made of hot-rolled parent material shows a change of the FWHM under cyclic loading for both load levels.

The results of residual stress relaxation are summarized in Fig. 9. The error bar shows the lower and upper limit of the measured residual stresses. In general, it is known that the residual stress relaxation under cyclic loading correlated with the maximum applied stress (peak stress) [31]. In this investigation, it is shown that the high load level—corresponding to the upper limit of the high cycle fatigue regime—leads to similar residual stress states for all investigated conditions after $N = 10{,}000$ load cycles.

5. Fatigue tests

5.1. *Fatigue test set-up*

Fatigue tests were carried out under axial loading on a horizontal resonance testing machine at a frequency around 33 Hz and a stress ratio $R = \sigma_{min}/\sigma_{max} = 0$. For each series, at least ten specimens were tested. Failure is defined as full fracture of a specimen.

5.2. *Geometrical properties of test specimens*

Before the actual fatigue tests, the test specimen weld geometry was determined including angular and axial misalignment. The goal of this investigation was to determine, whether geometrical differences may be responsible for differences in mechanical properties. For the local weld geometry measurements, laser triangulation was used and the point data was analysed using the curvature method, see Schubnell et al. [32] and Renken et al. [33]. The test specimen geometry

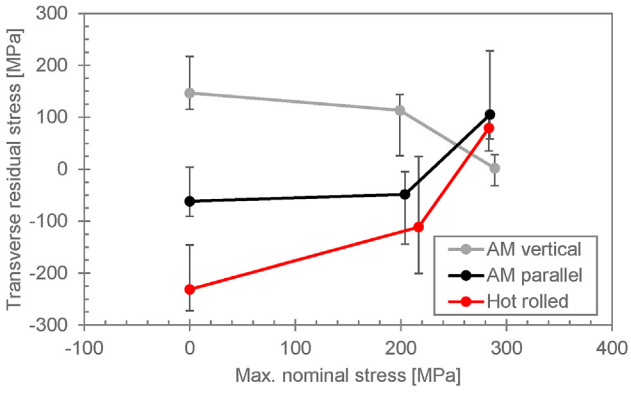

Fig. 9 – Residual stress level in dependency of the applied max. nominal stress after $N = 10{,}000$ load cycles.

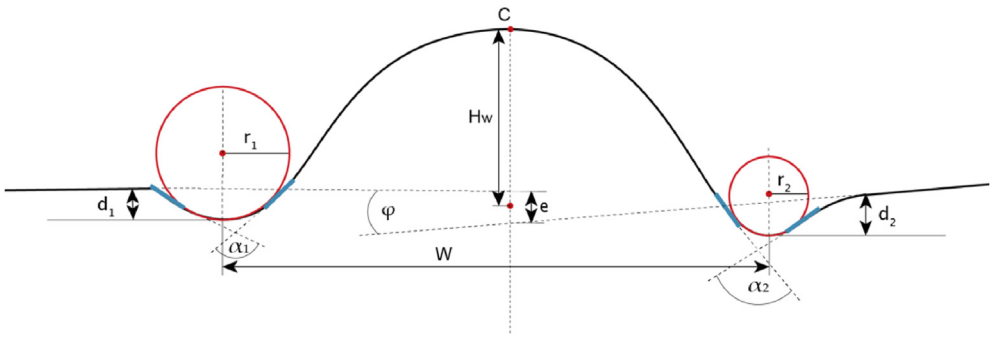

Fig. 10 – Schematic presentation of the test specimen geometry parameters [34].

and the local weld geometry parameters are schematically presented in Fig. 10.

For a statistical presentation of the geometrical data, each specimen surface is cut into 300 slices (0.1 mm steps), for which the local weld geometry is measured. The distributions of geometrical parameters are given in Fig. 11 separately for top and bottom side. The triangle in each distribution represents the median value.

The median weld toe radii on the top side were in all cases around 1 mm and slightly larger on the top side. The distributions for the weld toe radii seam to follow a lognormal distribution, which agrees well with many recent investigations, see e.g., [35,36]. The notch opening angles varied between 5° and 40°, and 5° and 50° on the top and bottom side, respectively. The undercut depths are similar for all three series and both sides, and in general quite low. In addition to the geometrical parameters, axial and angular misalignment of all joints was measured prior to testing. The ratio of axial misalignment to plate thickness e/t was smaller than 10% for all joints. Also, the absolute values of angular misalignment were below 1° for all specimens. Based on the geometrical properties, no difference in fatigue strength is expected for the three test series.

5.3. *Fatigue test results*

The fatigue test results are presented in Fig. 12 together with stress-life (S–N) curves. Tests reaching ten million cycles without failure were terminated and classified as run-outs (marked by arrows in Fig. 9). The test evaluation was performed by linear regression with:

$$N_f = 2 \times 10^6 \left(\frac{\Delta\sigma_n}{\Delta\sigma_R}\right)^{-k} \quad (3)$$

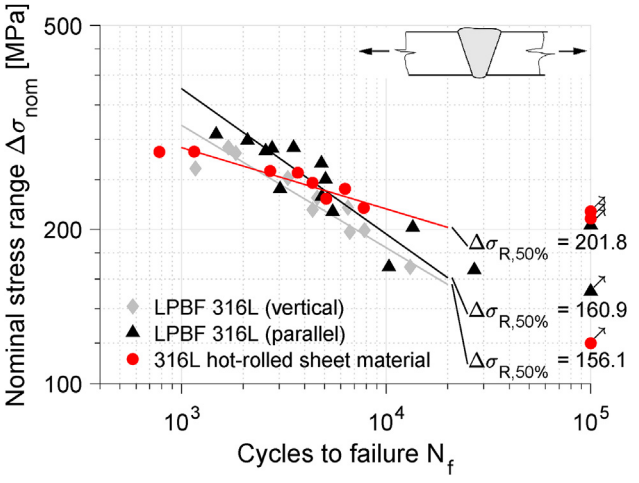

Fig. 12 – Fatigue assessment results of the butt joint fatigue test specimens.

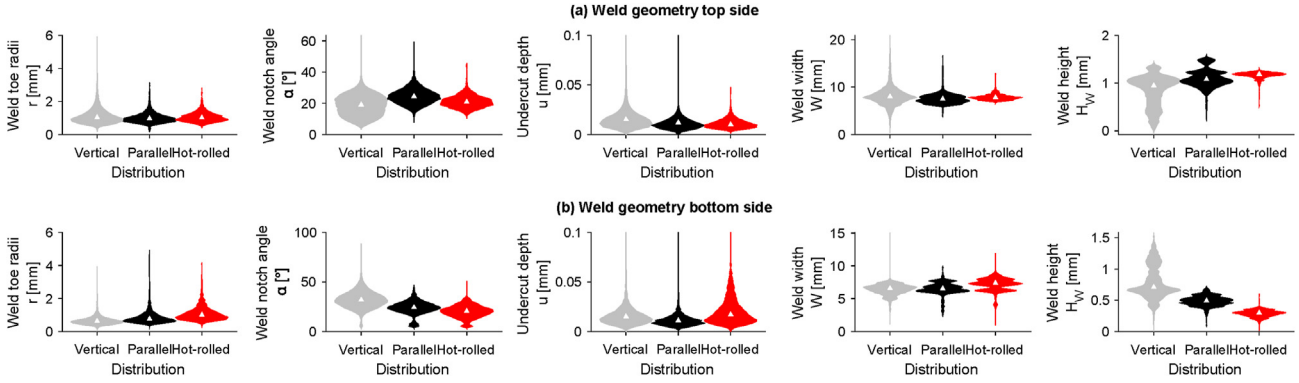

Fig. 11 – Results of the geometry measurements of the three different weld configurations.

where N_f is the endured number of cycles on the nominal stress range level $\Delta\sigma_n$, $\Delta\sigma_R$ is the reference fatigue strength at 2×10^6 cycles, and k the free inverse slope.

Besides the mean fatigue $\Delta\sigma_{R,50\%}$, the results for mean minus two standard deviation fatigue strength $\Delta\sigma_{R,97.7\%}$ (survival probability of $P_s = 97.7\%$), the scatter range T_σ between 2.3% and 97.7% survival probability as well as the inverse slope k are presented in Table 7.

All three test series exceed the fatigue design class (FAT) FAT90 for butt welded joints according to the recommendations of the International Institute of Welding (IIW) [37]; yet, the fatigue behaviour varies between the test series. Clearly, the butt joints made from conventionally hot-rolled steel plates show a shallower S–N curve slope and a higher fatigue strength at 2×10^6 cycles. Towards the low-cycle fatigue regime, the fatigue strength of the hot-rolled specimens is lower than for the two series made by LPBF process. A similar behaviour was observed in previous studies on notched specimens made by LBPF and cut from the same hot-rolled plate, see [3–5]. Interestingly, the slopes of both LPBF butt joint test series are similar, but a higher fatigue strength is observed for the specimens with layer orientation parallel to the weld seam.

For all test series, the knee point of the S–N curves is reached at around 1 million cycles, which is not unusual in joints with low notch acuity, see [38]. In LPBF specimens, small defects may lead to fatigue failure even after reaching the knee point at around 1 million cycles. Thus, a lower fatigue strength is not surprisingly. This is also reflected by the difference in slope of the S–N curves. Typically, welded joints of thin plates show a shallower slope than joints with thickness $t > 7$ mm, see [39]. This is, for example, the case for the hot-rolled plates.

In addition, the lower yield strength of the rolled sheet material may lead to lower fatigue strength towards the low-cycle fatigue regime, as local plastic strain ranges are more harmful. Thus, the tendency to lower fatigue strength of the rolled specimens around and below $N_f = 10^5$ cycles compared to the LPBF samples is not surprising.

In consequence, the difference in fatigue strength and S–N curves is thought to be related to difference in static strength, residual stress level, and possibly small crack-like defects. The latter hypothesis is subsequently investigated by means of fractographical analysis.

5.4. *Fractographical analysis*

Microscope (SEM) analyses were performed under a magnification between ×12 and ×500 at single specimens to detect locations of crack initiation (crack starter). In total, the fracture surface of two specimen in hot-rolled condition and of two specimens in AM vertical condition were investigated. Fig. 13 shows one fracture surface for each condition. In hot-rolled condition, see Fig. 13(a), multiple crack starters were determined over the entire area of the surface of final fracture (exemplarily displayed in Fig. 13(a) (Pos. 1 and Pos. 2)). In the investigated cases, failure location was always determined at the bottom side. Further investigations under a higher magnification of ×500 show that crack initiation occur in every investigated case from secondary notches at the weld toe (undercuts), see Fig. 13(a) (Pos. 1.1 and 1.2).

The SEM investigations at the specimens in AM vertical condition showed a similar topography of the fracture surfaces, see Fig. 13(b); however, in the investigated cases the failure locations were determined at the weld top side and bottom side as well. Multiple crack starters were determined again from secondary notches at the weld toe, see Fig. 13(b) (Pos. 2 and Pos. 2.1). Furthermore, some crack starters from near surface internal defects (pores) are found, see Fig. 13 (Pos. 1 and Pos. 1.1). In a short distance to the surface (in this case around 100 μm), these internal defects led to additional crack starters. In some cases, however, such internal defects are found close to the surface without leading to crack initiation.

6. Discussion

Based on the SEM investigations, a similar failure behaviour of the specimens in hot-rolled and AM condition was observed; yet, in some cases, near surface internal defects (voids or pores) led to additional crack initiation in the AM specimens. They may influence crack propagation at an early state of fatigue life. In the present study, an interaction between competing near surface internal defects and secondary notches (undercuts) at the weld toe is strongly assumed. This agrees with previous comparisons of notched specimens made by LBPF and cut from the same hot-rolled plate, see [3–5,16].

The occurrence of additional internal defects can also explain the different fatigue life of the specimens in hot-rolled and AM conditions at low load levels. It is fair to assume that the higher number of potential defects in AM condition reduce the fatigue life of the specimens—in particular in the low stress region close to the knee point of the S–N curves. Despite the evidence, it is strongly recommended to perform further investigations to verify this result for other weld types and materials.

The XRD-measurements reveal a high influence of the parent material condition and AM building direction on the residual stress state at the parent material. Tensile residual stresses were measured perpendicular to the layer orientation (or in building direction); however, significantly below the parent material yield strength. In addition, a significant difference was observed vertical and parallel to the building direction, which agrees well with many observations, see, e.g., Wu et al. [13]. Tensile and compressive residual stresses may affect the fatigue performance of the parent material if superimposed with external stresses; however, it seems that the welding process releases these harmful tensile residual stresses as well as compressive residual stresses around the weld toe and leads to similar residual stress states for all investigated parent material conditions. It is well known that residual stress relaxation is related to the ratio of maximum stress to yield strength of the material. Thus, the highest degree of residual stress relaxation was observed for specimen made of hot-rolled parent material with significant lower yield strength compared to the AM parent materials, see Table 2.

Identical to the parent material, the yield and ultimate tensile strength of the welded LPBF material of vertical layer orientation are the highest, but the fracture strain is the lowest. For the butt joints of hot-rolled reference material, the fracture strain is the highest, but the yield strength is the

Table 7 – Results of the fatigue tests.

Test series	Slope exponent k	Mean fatigue strength $\Delta\sigma_{R,50\%}$ ($P_s = 50.0\%$) [MPa]	Characteristic fatigue strength $\Delta\sigma_{R,97.7\%}$ ($P_s = 97.7\%$) [MPa]	Scatter ratio $1/T_s$
Hot-rolled	8.35	201.8	187.7	1.16
AM parallel	3.52	160.9	132.3	1.48
AM vertical	4.19	156.1	136.1	1.32

lowest, and the tensile strength is between the two LPBF types. In general, the results of the welded joints confirm the results from the tensile tests of the parent material; however, it should be mentioned that only the monotonic tensile tests were performed. Cyclic softening or hardening could lead to differences regarding the cyclic yield strength. This value may differ from the static yield strength.

In addition, the difference in microstructure of the rolled sheet and LPBF parent material led to large difference in yield and ultimate strength with more than twice the yield strength of LPBF tensile specimens perpendicular to the building direction compared to the rolled sheet material. It is assumed that this has an effect on the fatigue behavior at high stress ranges; however, due to its good weldability LPBF 316L retains high strength and ductility after gas metal arc welding. This agrees well with a study by Sampath et al. [9] on tungsten inert gas welding of LPBF 316L.

Differences in fatigue strength due to geometrical variations are ruled out based on weld geometry assessment. To this goal, laser scans were performed for all specimens prior to the fatigue tests to determine the local weld geometry. By comparison, no significant difference in weld geometry were determined for the three different test series.

Finally, significant variations of mechanical properties (static and cyclic strength, Charpy V-notch impact toughness and residual stress relaxation) are determined for butt joints made by gas metal arc welding from conventionally manufactured and from LBPF sheet material. These variations are attributed to difference in micro-structural features, residual stress levels, and possibly small crack-like defects.

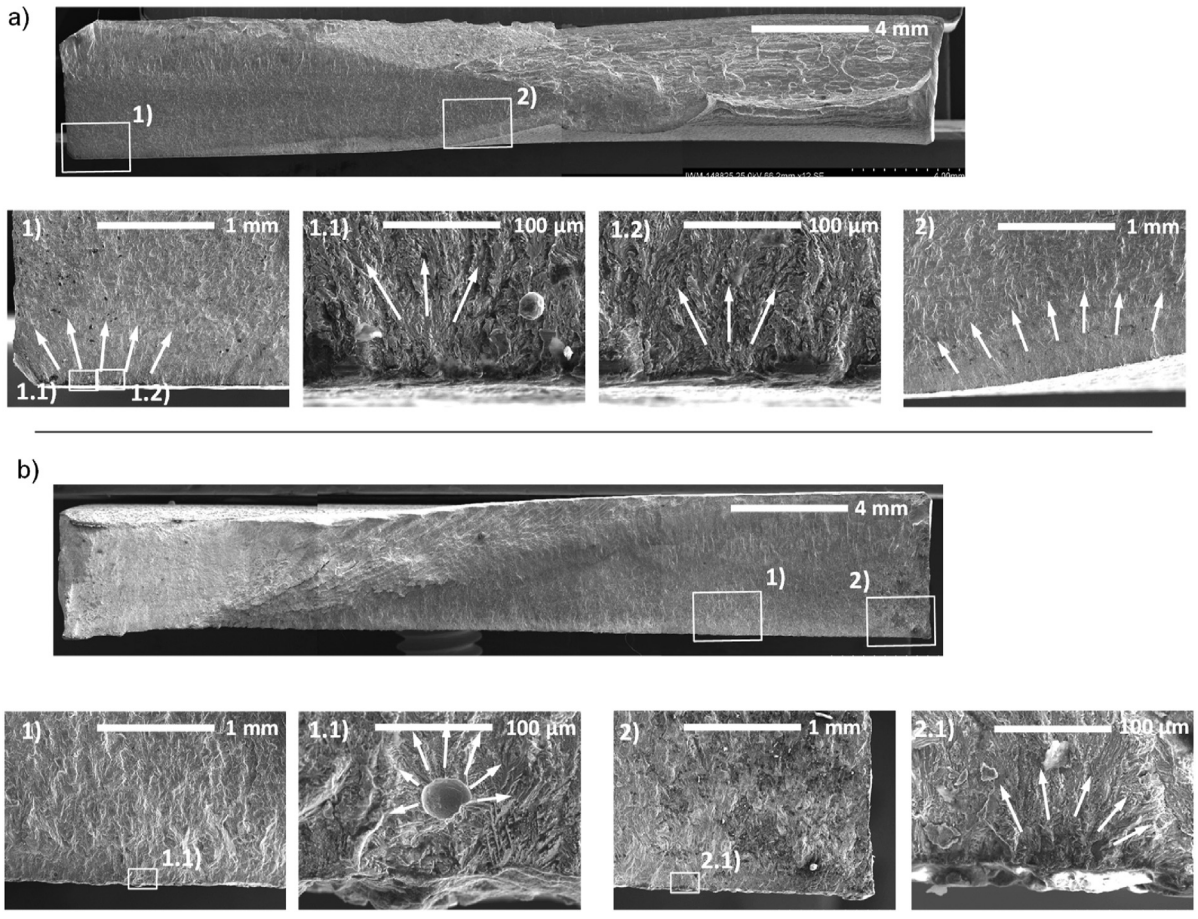

Fig. 13 – Fracture surface of welded specimen in hot-rolled condition (a) and in AM vertical condition (b).

7. Conclusion

Gas metal arc welding of 316L steel sheets made by laser powder bed fusion and hot rolling was performed to investigate the possibility to combine several additive manufactured parts due to a limited building volume. The residual stress states after welding were investigated by the cos α X-ray diffraction method. Three parent material conditions after welding were investigated: Hot-rolled steel plates, AM steel plates in vertical and horizontal building direction. From the investigation, the following conclusions are drawn:

- The LPBF material shows higher hardness in the parent material and welded joints compared to the hot-rolled reference joints, but lower Charpy V-notch impact toughness in the heat-affected zone.
- The building direction has a high influence on the residual stress state. In building direction, much higher tensile RS are determined than perpendicular to the building direction; however, a similar residual stress state was determined at the weld toe for all investigated parent material conditions. It is assumed that heating and cooling of the welding process leads to a relaxation of the residual stresses close to the weld.
- For a high load level (max. nominal stress >280 MPa) strong residual stress relaxation was determined for investigated parent material conditions. At low load levels (max. nominal stress <210 MPa) residual stress relaxation was determined for the specimen made of hot-rolled 316L steel. This behavior is expected to be related to differences in stress–strain behavior of the parent material and the welded joints.
- In summary, the yield and ultimate tensile strength of the welded LPBF material of vertical layer orientation are the highest, but the fracture strain is the lowest. In contrast, the butt joints of the hot-rolled reference material show the highest fracture strain. For the LPBF material of parallel layer orientation, the ultimate tensile strength is the lowest. In general, the results of the welded joints confirm the results from the tensile tests of the parent material. Also, the anisotropic behavior of the LPBF parent materials is confirmed by the tensile tests on welded joints.
- The butt joints made from conventionally hot-rolled steel plates show a shallower S–N curve slope and a higher fatigue strength at 2×10^6 cycles compared to the LPBF material with layer orientation parallel and vertical to the weld seam. Towards the low-cycle fatigue regime, the fatigue strength of the hot-rolled specimens is lower than for the two series made by LPBF process. The slope of both LPBF butt joint test series is similar, but a higher fatigue strength is observed for the specimens with layer orientation parallel to the weld seam.
- Based on the SEM investigations, a similar failure behaviour of the specimens in hot-rolled and AM condition was observed. In some cases, near-surface internal defects led to additional crack starters in the AM specimens. An interaction between competing near-surface internal defects and secondary notches at the weld toe is strongly assumed.

In summary, the variations in mechanical behaviour and in particular fatigue strength of conventionally and additively manufactured parts with butt joints made by gas metal arc welding is thought to be related to differences in microstructure, residual stress level, and possibly small crack-like defects; however, more research is required to reach a more thorough understanding of the interaction of the process–microstructure–property relation of welded AM components.

Funding information

This research did not receive any specific grant from funding agencies in the public, commercial, or not-for-profit sectors.

Declaration of competing interest

The authors declare that they have no known competing financial interests or personal relationships that could have appeared to influence the work reported in this paper.

REFERENCES

[1] Zapf H, Höfemann M, Emmelmann C. Laser welding of additively manufactured medium manganese steel alloy with conventionally manufactured dual-phase steel. Procedia CIRP 2020;94:655–60. https://doi.org/10.1016/J.PROCIR.2020.09.102.

[2] Möller B, Schnabel K, Scurria M, Jöckel A, Baumgartner J. Fatigue assessment of laser beam welds between AlSi10Mg AM-structures and conventionally manufactured aluminum by local approaches. Procedia Struct Integr 2021;34:160–5. https://doi.org/10.1016/J.PROSTR.2021.12.023.

[3] Braun M, Fassmer H, Rolof F, Müller AM, Ehlers S, Sheikhi S. Einfluss der Rissinitiierung und -ausbreitung auf die Schwingfestigkeit additiv und konventionell gefertigter Kerbproben aus austenitischem Stahl 316L. Berlin, Ger; 6. 2021. https://doi.org/10.48447/Add-2021-005.

[4] Braun M, et al. Fatigue strength of PBF-LB/M and wrought 316L stainless steel: effect of post-treatment and cyclic mean stress. Fatig Fract Eng Mater Struct 2021;44(11):3077–93. https://doi.org/10.1111/FFE.13552.

[5] Braun M, et al. Fatigue crack initiation and propagation in PBF-LB/M, WAAM and wrought 316L stainless steel after surface treatment. J Mater Res Technol 2022. under preparation.

[6] Geisen O, Müller V, Graf B, Rethmeier M. Integrated weld preparation designs for the joining of L-PBF and conventional components via TIG welding. Prog Addit Manuf 2022;7(5):811–21. https://doi.org/10.1007/s40964-021-00221-2.

[7] Brunner-Schwer C, Simón-Muzás J, Biegler M, Hilgenberg K, Rethmeier M. Laser welding of L-PBF AM components out of Inconel 718. Procedia CIRP 2022;111:92–6. https://doi.org/10.1016/J.PROCIR.2022.08.072.

[8] Jokisch T, Marko A, Gook S, Üstündag Ö, Gumenyuk A, Rethmeier M. Laser welding of SLM-manufactured tubes made of IN625 and IN718. Materials 2019;12(18):2967. https://doi.org/10.3390/MA12182967.

[9] Sampath VK, et al. 3d printing of stainless steel 316L and its weldability for corrosive environments. Mater Sci Eng, A 2022;833:142439. https://doi.org/10.1016/J.MSEA.2021.142439.

[10] Jiang W, et al. Fatigue life prediction of 316L stainless steel weld joint including the role of residual stress and its evolution: experimental and modelling. Int J Fatig 2021;143:105997. https://doi.org/10.1016/J.IJFATIGUE.2020.105997.
[11] Abbaszadeh M, et al. Numerical investigation of the effect of rolling on the localized stress and strain induction for wire + arc additive manufactured structures. J Mater Eng Perform 2019;28(8):4931–42.
[12] Guo D, et al. Solidification microstructure and residual stress correlations in direct energy deposited type 316L stainless steel. Mater Des 2021;207:109782. https://doi.org/10.1016/j.matdes.2021.109782.
[13] Wu AS, Brown DW, Kumar M, Gallegos GF, King WE. An experimental investigation into additive manufacturing-induced residual stresses in 316L stainless steel. Metall Mater Trans A Phys Metall Mater Sci 2014;45(13):6260–70. https://doi.org/10.1007/s11661-014-2549-x.
[14] Braun M, et al. Fatigue strength of PBF-LB/M and wrought 316L stainless steel: effect of post-treatment and cyclic mean stress. Fatig Fract Eng Mater Struct 2021;44(11):3077–93. https://doi.org/10.1111/FFE.13552.
[15] Schubnell J, Sarmast A, Altenhöner F, Sheikhi S, Braun M, Ehlers S. Residual stress analysis of butt welds made of additive an tradionally manufactured 316L stainless steel plates. ICRS11 – 11th International Conference on Residual Stresses. France, Nancy; 2022.
[16] Taghipour A, et al. Strengthening mechanisms and strain hardening behavior of 316L stainless steel manufactured by laser-based powder bed fusion. Adv Eng Mater 2022:2201230. https://doi.org/10.1002/ADEM.202201230.
[17] DebRoy T, et al. Additive manufacturing of metallic components – process, structure and properties. Prog Mater Sci 2018;92:112–224. https://doi.org/10.1016/J.PMATSCI.2017.10.001.
[18] Liu L, et al. Dislocation network in additive manufactured steel breaks strength–ductility trade-off. Mater Today 2018;21(4):354–61. https://doi.org/10.1016/J.MATTOD.2017.11.004.
[19] Wang YM, et al. Additively manufactured hierarchical stainless steels with high strength and ductility. Nat Mater 2017;17(1):63–71. https://doi.org/10.1038/nmat5021.
[20] Taira S, Tanaka K, Yamasaki T. A method of X-ray microbeam measurement of local stress an its application to fatigue crack growth problems. J Soc Mater Sci 1978;27:251–6. 294.
[21] Müller P, Macherauch E. Das sin 2 ψ-Verfahren der röntgenographischen Spannungsmessung. Z Angew Phys 1961;13:305–12.
[22] Sasaki T, Sato H. X-ray stress measurement of austenitic stainless steel with cosα method and two-dimensional X-ray detector. Mater Sci Forum 2017;879:1679–84. https://doi.org/10.4028/www.scientific.net/MSF.879.1679.
[23] Miyazaki T, Sasaki T. X-ray residual stress measurement of austenitic stainless steel based on fourier analysis. Nucl Technol 2016;194(1):111–6. https://doi.org/10.13182/NT15-25. American Nuclear Society.
[24] Tanaka K. The cosα method for X-ray residual stress measurement using two-dimensional detector. Mech Eng Rev 2019;6(1). https://doi.org/10.1299/mer.18-00378. 18-00378-18-00378.
[25] Nitschke-Pagel T. Recommendations for the measurement of residual stresses in welded joints by means of X-ray diffraction—results of the WG6-RR test. Weld World 2021;65(4):589–600. https://doi.org/10.1007/S40194-020-01029-4/FIGURES/12.
[26] Spieß L, Teichert G, Schwarzer R, Behnken H, Genzel C. Röntgenographische Spannungsanalyse. Mod Röntgenbeugung 2019:325–406. https://doi.org/10.1007/978-3-8348-8232-5_10.
[27] Hensel J, Nitschke-Pagel T, Dilger K. Engineering model for the quantitative consideration of residual stresses in fatigue design of welded components. Weld World 2017;61(5):997–1002. https://doi.org/10.1007/s40194-017-0467-4.
[28] Hensel J. Mean stress correction in fatigue design under consideration of welding residual stress. Weld World 2020;64(3):535–44. https://doi.org/10.1007/s40194-020-00852-z.
[29] Vashista M, Paul S. Correlation between full width at half maximum (FWHM) of XRD peak with residual stress on ground surfaces. Mater Sci 2012;92(33):4194–204. https://doi.org/10.1080/14786435.2012.704429.
[30] Vashista M, Yusufzai MZK. Correlation between full width at half maximum (FWHM) of XRD peak with mechanical properties. Int J Metall Alloy 2015;1(1):15–23.
[31] Schulze V. Modern mechanical surface treatment: states, stability, effects. New York: Wiley VCH; 2006.
[32] Schubnell J, et al. Influence of the optical measurement technique and evaluation approach on the determination of local weld geometry parameters for different weld types. Weld World 2020;64(2):301–16. https://doi.org/10.1007/s40194-019-00830-0.
[33] Renken F, et al. An algorithm for statistical evaluation of weld toe geometries using laser triangulation. Int J Fatig 2021;149:106293. https://doi.org/10.1016/J.IJFATIGUE.2021.106293.
[34] Braun M, Kellner L, Schreiber S, Ehlers S. Prediction of fatigue failure in small-scale butt-welded joints with explainable machine learning. Proced Struct Integr 2021. https://doi.org/10.1016/j.prostr.2022.03.019.
[35] Schork B, et al. The effect of the local and global weld geometry as well as material defects on crack initiation and fatigue strength. Eng Fract Mech 2017;198:103–22. https://doi.org/10.1016/j.engfracmech.2017.07.001.
[36] Braun M, et al. Statistical characterization of stress concentrations along butt joint weld seams using deep neural networks. Appl Sci 2022;12(12):6089. https://doi.org/10.3390/APP12126089.
[37] Hobbacher AF. Recommendations for fatigue Design of welded Joints and components, 2th illust. Springer; 2016.
[38] Braun M, Fischer C, Baumgartner J, Hecht M, Varfolomeev I. Fatigue crack initiation and propagation relation of notched specimens with welded joint characteristics. Metals 2022;12(4):615. https://doi.org/10.3390/MET12040615.
[39] Baumgartner J, Hobbacher AF, Rennert R. Fatigue assessment of welded thin sheets with the notch stress approach – proposal for recommendations. Int J Fatig 2020;140:105844. https://doi.org/10.1016/J.IJFATIGUE.2020.105844.